JOURNAL OF SOLID STATE CHEMISTRY 120, 364–371 (1995)

The Al-Rich Part of the System $CaO–Al_2O_3–MgO$

Part II. Structure Refinement of Two New Magnetoplumbite-Related Phases

Nobuo Iyi,* Matthias Göbbels,† and Yoshio Matsui*

*National Institute for Research in Inorganic Materials, Namiki 1-1, Tsukuba-shi, Ibaraki 305, Japan; and †Institut für Kristallographie, RWTH Aachen, Jägerstrasse 17-19, 52056 Aachen, Germany

Received February 23, 1995; revised May 8, 1995; accepted May 9, 1995

Crystals of two new phases, which were recently found in the system $CaO–Al_2O_3–MgO$ lying on the join connecting calcium hexaaluminate ($CaAl_{12}O_{19}$) of the magnetoplumbite structure and spinel ($MgAl_2O_4$), were grown by the floating zone method. The stoichiometric formulas for these two phases can be given as $Ca_2Mg_2Al_{28}O_{46}$ (CAM-I) and $CaMg_2Al_{16}O_{27}$ (CAM-II). On the basis of the stacking sequence revealed by high-resolution electron microscopy, the structure models were made, and further, the structure refinement was conducted by using single crystal X-ray diffraction data. It was shown that both phases have magnetoplumbite-related structures composed of two types of structure units, $M(CaAl_{12}O_{19}$; magnetoplumbite unit) and $S(Mg_2Al_4O_8$; spinel unit), and that the stacking sequences are $(M_2S)_n$ for CAM-I (c = 79.810 Å) and $(MS)_n$ for CAM-II (c = 31.288 Å). In the terminology of hexagonal ferrite structure system, CAM-I is of the "X-type structure" with space group $R\bar{3}m$ and CAM-II is of the "W-type structure" with $P\bar{6}m2$ symmetry.

INTRODUCTION

Alkaline-earth oxides such as CaO and SrO are known to form hexagonal aluminates having magnetoplumbite or related structures in the binary system with Al_2O_3 (1–3). The general chemical formula of the magnetoplumbite-type hexaaluminates can be expressed as $GAl_{12}O_{19}$, where G represents a large cation such as Ca^{2+} and Sr^{2+}. This structure consists of two kinds of layers, which stack alternately in the c direction exhibiting hexagonal symmetry. The layer containing a large cation G has been referred to as "the mirror plane" or "the conduction plane," and the other layer, having a spinel structure, as "the spinel block" (4). The small divalent cation Mg^{2+} is also incorporated, however, not in the conduction plane, but in the spinel block by replacing trivalent Al^{3+} ions. The difference of their ionic valences is known to cause some kind of charge compensation or sometimes modification of the structure (5).

In the case of the binary system $CaO–Al_2O_3$, Ca-hexaaluminate was already confirmed to have a magnetoplumbite structure with the formula $CaAl_{12}O_{19}$ by the single crystal diffraction method (2, 3), but the effects of adding as a third component MgO have not been well established. Stevels and Schrama-de Pauw (5) assumed MgO-incorporated Ca–hexaaluminate as "$CaMg_xAl_{12-2x/3}O_{19}$," which implied the existence of some vacancies in the magnetoplumbite structure. Kumar and Kay (6) and Fay and Kumar (7) presumed the structure, but without any structural refinement.

Recently, Göbbels *et al.* (8) studied the phase relation in the Al-rich part of the system $CaO–Al_2O_3–MgO$ and found two new compounds by using powder sintering, optical microscopy, EPMA (electron probe microanalysis), and X-ray powder diffraction. As indicated in the phase diagram shown in the Part I of the series of our papers (8), these compounds are situated on the join connecting calcium–hexaaluminate ($CaAl_{12}O_{19}$), which has a magnetoplumbite structure, and spinel ($MgAl_2O_4$). The Ca-rich compound was denoted as "CAM-I" and the Mg-rich compound as "CAM-II." The preliminary powder diffraction data suggested that the structures are closely related to the magnetoplumbite, though their c-axis lengths were much larger than those of the normal hexaaluminates. The structure determination from powder X-ray data was not successful. So, single crystal growth of these new compounds was attempted since single crystals are necessary for further structure analysis such as single crystal X-ray diffraction and electron microscopy. Recently we succeeded in growing them by the floating zone (FZ) method.

The purpose of the present paper is to reveal the structures of two new compounds related to hexaaluminates in the ternary system $CaO–Al_2O_3–MgO$ by using electron microscopy and single crystal X-ray diffraction methods.

EXPERIMENTS

Crystal Growth

Starting materials were the high purity reagents $CaCO_3$, MgO, and Al_2O_3 (99.9% Merk). They were mixed mechani-

0022-4596/95 $12.00

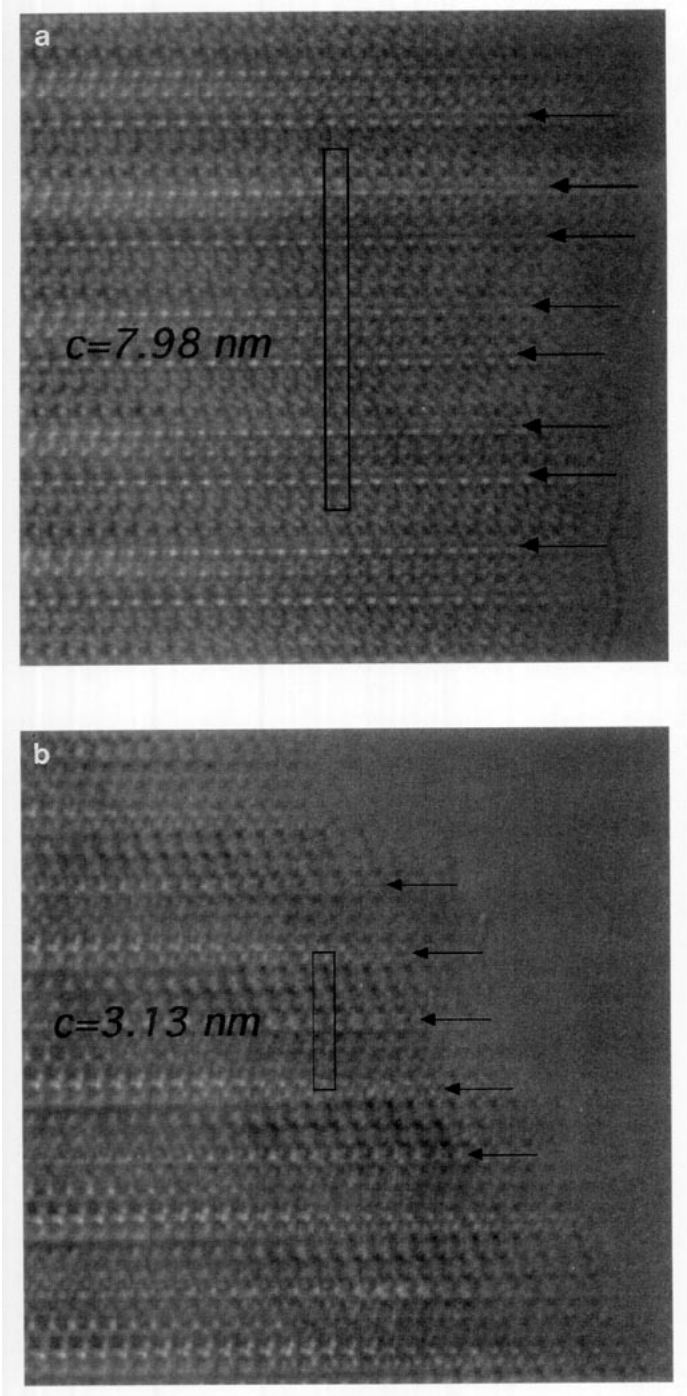

FIG. 1. HRTEM pictures of (a) CAM-I and (b) CAM-II projected along the [100] direction, revealing the stacking sequences. Arrows show the conduction planes containing Ca ions.

cally in an agate mortar under acetone in the stoichiometric ratio for each compound and in the corresponding ratio for coexisting melts. The homogenized batches were calcined at 1100°C to ensure the decomposition of $CaCO_3$. The rods of suitable size, which had been pressed hydrostatically, were sintered in a molybdenum wound resistance furnace at 1700°C in an oxygen atmosphere. Due to the incongruently melting nature of the compounds, the FZ crystal growth method was applied (9). The apparatus was of the infrared radiation convergence type (Nichiden Machinery Ltd., NEC) with a xenon lamp used as the heat source. A sintered pellet of melt composition was placed between the rods. The growth rate was 2 mm/hr and air was used as the atmosphere during growth. After being cut, the resulting crystals were served for electron microscopy, X-ray diffraction, and EPMA (JEOL JXA-8600).

Electron Microscopy

The crystals were ground in CCl_4 using an agate mortar and then dispersed on holey carbon films supported by copper grids. High-resolution transmission electron microscope (HRTEM) observations were made by the Hitachi H-1500 machine operated at 800 kV (10). Crystal fragments with the *a* axis parallel to the electron beam directions were selected and HRTEM images were recorded at magnification of approximately 500,000 times.

X-Ray Data Collection

CAM-I. Specimens were cut and the selected cube was ground to a sphere with radius about 90 μm and used for X-ray diffraction. The crystallinity and symmetry were checked by the X-ray photographic methods. The precession photos revealed that CAM-I belonged to the rhombohedral crystal system. Reflections with $-h + k + l = 3n$ for *hkl* and $l = 2n$ for *hhl* were observed. No evidence of superstructure was found. Specimens were mounted on

TABLE 1
Crystallographic Data of CaMg–Hexaaluminates

	CAM-I	CAM-II
Symmetry	Rhombohedral	Hexagonal
Space group	$R\bar{3}m$	$P\bar{6}m2$
Cell const.	a = 5.573(1)Å	a = 5.590(2)Å
	c = 79.810(2)Å	c = 31.288(1)Å
	V = 2146.5 Å^3	V = 846.8 Å^3
	Z = 3	Z = 2
Formula[a]	$Ca_{2.00}Mg_{1.41}Al_{28.4}O_{46}$	$Ca_{0.98}Mg_{1.31}Al_{16.5}O_{27}$
Formula (ideal)	$Ca_2Mg_2Al_{28}O_{46}$	$Ca_1Mg_2Al_{16}O_{27}$
Structure type	X type	W type
Stacking[b]	$(M_2S)_n$	$(MS)_n$
Independent reflections	586	640
R factor	4.7%	5.7%
2θ range	2θ = 3°–53°	2θ = 3°–70°
Data collection	ω scan	ω scan

[a] Experimental, by EPMA.
[b] Stacking elements: $M = CaAl_{12}O_{19}$ and $S = Mg_2Al_4O_8$.

TABLE 2
The Positional and Thermal Parameters of CaMg–Hexaaluminate (CAM-I) Obtained by the X-Ray Single Crystal Diffraction Method

		Positional parameters[a]		Thermal parameters[b] × 10^4					
Atom	Site	x	z	U_{11}	U_{33}	U_{12}	U_{13}	U_{23}	B_{eq}[c]
Ca	6*c*	0	0.09817(4)	164(12)	151(17)	$1/2U_{22}$	0	0	1.26
Al(1)	18*h*	0.16498(24)	0.05925(2)	47(12)	47(10)	17(18)	2(8)	$-U_{13}$	0.39
Al(2)	18*h*	0.16478(24)	0.13682(2)	48(12)	58(98)	26(18)	3(9)	$-U_{13}$	0.40
Al(3)	9*e*	1/2	0	110(16)	149(15)	$1/2U_{22}$	149(16)	$2U_{13}$	1.23
Al(4)	6*c*	0	0.02230(5)	94(15)	58(19)	$1/2U_{22}$	0	0	0.65
Al(5)	6*c*	0	0.36223(5)	85(14)	30(20)	$1/2U_{22}$	0	0	0.53
Al(6)	6*c*	0	0.29652(6)	120(15)	194(24)	$1/2U_{22}$	0	0	1.15
Al(7)	6*c*	0	0.25133(5)	56(14)	28(18)	$1/2U_{22}$	0	0	0.37
Al(8)	6*c*	0	0.43231(6)	50(15)	452(33)	$1/2U_{22}$	0	0	1.45
Al(9)	6*c*	0	0.21891(5)	62(14)	34(18)	$1/2U_{22}$	0	0	0.42
Al(10)	6*c*	0	0.17454(5)	45(13)	51(18)	$1/2U_{22}$	0	0	0.37
Al(11)	3*b*	0	1/2	46(18)	28(26)	$1/2U_{22}$	0	0	0.31
O(1)	18*h*	0.17866(55)	0.01406(6)	97(31)	151(26)	64(48)	41(21)	$-U_{13}$	0.86
O(2)	18*h*	0.48735(52)	0.04348(6)	63(28)	108(24)	27(44)	−9(21)	$-U_{13}$	0.63
O(3)	18*h*	0.83405(52)	0.07007(5)	85(29)	99(25)	54(46)	−22(21)	$-U_{13}$	0.66
O(4)	18*h*	0.51437(51)	0.09804(5)	56(27)	42(24)	−21(45)	1(22)	$-U_{13}$	0.57
O(5)	18*h*	0.83718(50)	0.12569(5)	52(25)	43(22)	6(43)	18(21)	$-U_{13}$	0.45
O(6)	18*h*	0.48801(52)	0.15222(5)	70(29)	92(24)	54(44)	9(20)	$-U_{13}$	0.54
O(7)	6*c*	0	0.31962(11)	100(34)	149(50)	$1/2U_{22}$	0	0	0.92
O(8)	6*c*	0	0.04541(11)	59(31)	88(46)	$1/2U_{22}$	0	0	0.54
O(9)	6*c*	0	0.40319(10)	65(31)	30(44)	$1/2U_{22}$	0	0	0.42
O(10)	6c	0	0.45877(10)						0.19
O(11)	6*c*	0	0.15161(11)	51(31)	76(46)	$1/2U_{22}$	0	0	0.47

[a] $y = 2x$.
[b] The temperature factor is expressed as: $\exp(-2\pi^2(h^2a^{*2}U_{11} + k^2b^{*2}U_{22} + l^2c^{*2}U_{33} + 2hka^*b^*U_{12} + 2hla^*c^*U_{13} + 2klb^*c^*U_{23})$. $U_{22} = U_{11}$.
[c] $B_{eq} = \frac{4}{3}(\sum_i \sum_j B_{ij}\mathbf{a}_i\mathbf{a}_j) = \frac{8}{3}\pi^2(\sum_i \sum_j U_{ij})$.

the AFC-5 automatic four-circle diffractometer (Rigaku Co. Ltd.), and intensities were measured using graphite monochromatized Mo$K\alpha$ radiation (λ = 0.71068 Å) in a ω scanning mode up to $2\theta = 53°$. The scanning speed was 1° min^{-1} in ω. The space group $R\bar{3}m$ was assumed. All reflections with $-h + k + l = 3n$ for hkl and $l = 2n$ for hhl of six asymmetric units were collected, and Lorentz polarization and absorption corrections were applied. Linear absorption coefficients were 16.4 cm^{-1} for CAM-I. Absorption due to the crystal shape was corrected. A set of six standard reflections was used for monitoring the fluctuation of the source X-ray intensity; however, no systematic intensity change was observed. Averaging of six equivalent reflections and omission of the reflections with $I < 3\sigma(I)$ gave the final set of nonzero independent reflections (a total of 586). Internal R factors within equivalent reflections were $R_{int} = \sum |F - \langle F\rangle|/\sum |F| = 0.007$ and $wR_{int} = \sum w|F - \langle F\rangle|/\sum w|F| = 0.006$. The $\sigma(F)$'s (of equivalent reflections) based on counting statistics were averaged and used for the weighting factor in the least-squares refinement ($w = 1/\sigma(F)^2$).

CAM-II. Rectangular crystals (180 × 140 × 135 μm) were used for X-ray diffraction. The crystallinity and symmetry were checked by the X-ray photographic methods, which revealed the crystal system to be hexagonal. Systematic absences and superstructure spots were not observed. On the four-circle diffractometer, intensities were measured using graphite monochromatized Mo$K\alpha$ radiation (λ = 0.71068 Å) in a ω scanning mode up to $2\theta = 70°$. The scanning speed was 1° min^{-1} in ω. The space group $P\bar{6}m2$ was assumed. All reflections of the four asymmetric units were collected, and the Lorentz polarization and absorption corrections were applied. The linear absorption coefficient was as low as 15.8 cm^{-1}, and the absorption due to the crystal shape was not corrected for. A set of six standard reflections was used for monitoring the fluctuation of the source X-ray intensity; however, no systematic intensity change was observed. The anomalous dispersion effect was not taken into account. Averaging of four equivalent reflections and omission of the reflections with $I < (3\sigma(I)$ gave the final set of nonzero independent reflections (a total of 640), with $R_{int} = 0.019$ and $wR_{int} = 0.020$. The

TABLE 3
The Positional and Thermal Parameters of CaMg–Hexaaluminate (CAM-II) Obtained by the X-Ray Single Crystal Diffraction Method

Atom	Site	Positional parameters[a]		Thermal parameters[b] × 10^4						
		x	z	U_{11}	U_{22}	U_{33}	U_{12}	U_{13}	U_{23}	B_{eq}[c]
Ca(1)[d]	1*a*	0	0	162(73)	U_{11}	248(56)	$1/2U_{22}$	0	0	1.5
Ca(2)	1*b*	0	1/2	146(62)	U_{11}	133(41)	$1/2U_{22}$	0	0	1.1
Al(1)	6*n*	0.1644(12)	0.09903(9)	35(44)	U_{11}	59(12)	18(68)	6(29)	$-U_{13}$	0.34
Al(2)	6*n*	0.5000(18)	0.24896(12)	115(16)	U_{11}	88(10)	50(26)	18(14)	$-U_{13}$	0.87
Al(3)	6*n*	0.8352(12)	0.40076(8)	40(43)	U_{11}	52(11)	1(68)	−8(31)	$-U_{13}$	0.42
Al(4)	2*g*	0	0.19150(23)							0.175(4)
Al(5)	2*g*	0	0.30423(26)	144(26)	U_{11}	54(28)	$1/2U_{22}$	0	0	0.90
Al(6)	2*h*	1/3	0.34300(28)	169(57)	U_{11}	116(35)	$1/2U_{22}$	0	0	1.2
Al(7)	2*h*	1/3	0.46073(24)	77(23)	U_{11}	81(29)	$1/2U_{22}$	0	0	0.63
Al(8)	2*h*	2/3	0.04303(22)							0.021(4)
Al(9)	2*i*	2/3	0.15450(26)	5(39)	U_{11}	111(35)	$1/2U_{22}$	0	0	0.32
Al(10)	2*i*	1/3	0.17647(26)	65(49)	U_{11}	7(26)	$1/2U_{22}$	0	0	0.36
Al(11)	2*i*	2/3	0.32407(26)	63(51)	U_{11}	68(31)	$1/2U_{22}$	0	0	0.51
Al(12)[e]	2*h*	1/3	0.00757(33)							0.33(2)
Al(13)[e]	2*i*	2/3	0.5060(11)	44(34)	U_{11}	156(206)	$1/2U_{22}$	0	0	0.64
O(1)	6*n*	0.8330(25)	0.07198(30)							0.791(5)
O(2)	6*n*	0.4862(22)	0.13922(23)							0.200(5)
O(3)	6*n*	0.1824(19)	0.21653(32)							0.692(5)
O(4)	6*n*	0.8225(20)	0.28716(26)							0.636(5)
O(5)	6*n*	0.5121(26)	0.35988(28)							0.934(6)
O(6)	6*n*	0.1637(20)	0.42960(26)							0.352(5)
O(7)	3*j*	0.5141(37)	0							0.987(9)
O(8)	3*k*	0.4855(31)	1/2							0.221(7)
O(9)	2*g*	0	0.1333(7)							0.622(11)
O(10)	2*g*	0	0.3652(7)							0.654(11)
O(11)	2*h*	1/3	0.0743(8)							1.00(1)
O(12)	2*h*	1/3	0.2872(6)							0.276(9)
O(13)	2*i*	2/3	0.2190(8)							0.872(12)
O(14)	2*i*	2/3	0.4308(7)							0.06(1)

[a] $y = 2x$.
[b] The temperature factor is expressed as: $\exp(-2\pi^2(h^2a^{*2}U_{11} + k^2b^{*2}U_{22} + l^2c^{*2}U_{33} + 2hka^*b^*U_{12} + 2hla^*c^*U_{13} + 2klb^*c^*U_{23})$.
[c] $B_{eq} = \frac{4}{3}(\Sigma_i \Sigma_j B_{ij}\mathbf{a}_i\mathbf{a}_j) = \frac{8}{3}\pi^2(\Sigma_i \Sigma_j U_{ij})$.
[d] Occupancy: 93%.
[e] Occupancy: 50%.

$\sigma(F)$'s based on counting statistics (of equivalent reflections) were averaged and used for the weighting factor in the least-squares refinement ($w = 1/\sigma(F)^2$).

Refinement

The neutral scattering factors were taken from Ref. (11). The full matrix least-squares program used was a modified version of RSFLS-4 (12) and Fourier syntheses were done using RSSFR-5 (13). Secondary extinction corrections based on the algorithm of Becker and Coppens (14, 15) were applied to the refinement of CAM-I by using the extinction parameters g (mosaic distribution).

The lattice parameters of both compounds were also determined on the basis of 2θ data (20–25 reflections with a 2θ range of 50°–90°, Mo$K\alpha_1$ radiation, $\lambda = 0.70926$ Å) collected on the four-circle diffractometer.

RESULTS AND DISCUSSION

The resultant HRTEM images of both compounds are shown in Fig. 1, where positions of the conduction planes are indicated by arrows. The spinel-type blocks were separated by the conduction planes. These HRTEM data suggest that CAM-I has alternate stackings of normal ($ACBA$) and extended ($ACBACB$) spinel blocks and that CAM-II has only extended spinel blocks (Here, A, B, and C indicate oxygen packing.). These kinds of stackings were already reported in the series of mixed-layer structures of so-called hexagonal ferrites or "hexaferrites" (16, 17), and, in the

TABLE 4
Interatomic Distances of CAM-I

		Number of bonds	Distance (Å)
	Octahedral coordination		
Al(1)	–O(3)	2	1.815(4)
	–O(9)	1	1.832(4)
	–O(8)	1	1.938(5)
	–O(2)	2	2.005(4)
Al(2)	–O(5)	2	1.814(4)
	–O(10)	1	1.863(4)
	–O(11)	1	1.981(6)
	–O(6)	2	1.990(4)
Al(3)	–O(1)	4	1.917(4)
	–O(7)	2	1.946(6)
Al(5)	–O(2)	3	1.888(4)
	–O(1)	3	1.906(4)
Al(7)	–O(3)	3	1.875(3)
	–O(4)	3	1.949(4)
Al(9)	–O(5)	3	1.876(3)
	–O(4)	3	1.967(4)
Al(11)	–O(6)	6	1.886(3)
	Tetrahedral coordination		
Al(4)	–O(8)	1	1.844(10)
	–O(1)	3	1.846(2)
Al(6)	–O(2)	3	1.811(2)
	–O(7)	1	1.843(10)
Al(10)	–O(6)	3	1.802(2)
	–O(11)	1	1.830(10)
	Polyhedron 5-coordinated		
Al(8)	–O(4)	3	1.749(1)
	–O(10)	1	2.112(10)
	–O(9)	1	2.324(10)
	Polyhedron 12-coordinated		
Ca	–O(5)	3	2.701(4)
	–O(3)	3	2.756(4)
	–O(4)	6	2.790(3)

TABLE 5
Interatomic Distances of CAM-II

		Number of bonds	Distance (Å)
	Octahedral coordination		
Al(1)	–O(1)	2	1.814(13)
	–O(11)	1	1.810(11)
	–O(9)	1	1.920(12)
	–O(2)	2	2.007(11)
Al(2)	–O(3)	2	1.847(12)
	–O(13)	1	1.866(13)
	–O(4)	2	1.968(12)
	–O(12)	1	2.010(12)
Al(3)	–O(6)	2	1.830(8)
	–O(14)	1	1.883(8)
	–O(10)	1	1.955(9)
	–O(5)	2	2.024(13)
Al(7)	–O(6)	3	1.909(6)
	–O(8)	3	1.918(5)
Al(8)	–O(7)	3	1.999(5)
	–O(1)	3	1.847(6)
Al(10)	–O(2)	3	1.884(7)
	–O(3)	3	1.925(8)
Al(11)	–O(5)	3	1.870(8)
	–O(4)	3	1.900(7)
	Tetrahedral coordination		
Al(4)	–O(9)	1	1.820(22)
	–O(3)	3	1.932(5)
Al(5)	–O(4)	3	1.800(4)
	–O(10)	1	1.907(23)
Al(6)	–O(12)	1	1.745(21)
	–O(5)	3	1.809(4)
Al(9)	–O(2)	3	1.812(3)
	–O(13)	1	2.018(25)
	Polyhedron 5-coordinated		
Al(12)	–O(7)	3	1.767(2)
	–O(11)	1	2.087(29)
	–O(11)′	1	2.561(29)
Al(13)	–O(8)	3	1.764(4)
	–O(14)	1	1.975(39)
	–O(14)′	1	2.352(39)
	Polyhedron 12-coordinated		
Ca(1)	–O(1)	6	2.773(8)
	–O(7)	6	2.799(21)
Ca(2)	–O(6)	6	2.714(7)
	–O(8)	6	2.799(18)

terminology used in the hexaferrite system, CAM-I corresponds to the stacking of X-type, and CAM-II to that of W-type. In the case of hexaferrites, the content of the conduction planes are of magnetoplumbite-type, but HRTEM is not enough for the clarification of the content of the conduction layer of our compounds. Further structure refinements were, therefore, conducted by using the single crystal X-ray diffraction data. The starting parameters for the least-square refinement were calculated on the basis of this stacking information. The refinements were conducted with checking the difference Fourier maps and the final anisotropic refinement converged successfully to yield $R = \sum \| |F_o| - |F_c| \| / \sum |F_o| = 0.047$ ($wR = (\sum w(|F_o| - |F_c|)^2 / \sum w|F_o|^2)^{1/2} = 0.054$, $S = [\sum w(|F_o| - |F_c|)^2 / (m\text{-}n)]1/2 = 7.5$) for CAM-I, and $R = 0.057$ ($wR = 0.057$, $S = 8.0$) for CAM-II. Maximum residual electron density in the final difference Fourier maps were +2.4 e/Å^3 at (2/3, 1/3, 0.03) and −1.3 e/Å^3 at (0, 0, 0.07) for CAM-I, and +3.4 e/Å^3 at (2/3, 1/3, 0.12) and −1.4 e/Å^3 at (0, 0, 0) for CAM-II, respectively. Table 1 shows the crystallographic data of both phases, together with the data collection conditions as well as the final R values. Positional parameters, bond lengths, and angles for CAM-I are listed in Tables 2, 4, and 6, respectively. Tables 3, 5, and 7 show the corresponding parameters for CAM-II. The result showed that the structure of the condition layer is of magnetoplumbite type, in which there are face-sharing Al octa-

TABLE 6
Interatomic Angles of CAM-I

	Number of bonds	Angle (°)
Octahedral coordination		
O(2)–Al(1) –O(2)′	1	79.90(14)
O(2)–Al(1) –O(3)	2	89.97(12)
O(2)–Al(1) –O(8)	2	90.19(20)
O(2)–Al(1) –O(9)	2	84.28(19)
O(3)–Al(1) –O(3)′	1	99.66(16)
O(3)–Al(1) –O(8)	2	85.00(17)
O(3)–Al(1) –O(9)	2	99.61(18)
O(5)–Al(2) –O(5)′	1	97.27(15)
O(5)–Al(2) –O(6)	2	90.64(11)
O(5)–Al(2) –O(10)	2	98.56(18)
O(5)–Al(2) –O(11)	2	86.30(16)
O(6)–Al(2) –O(6)′	1	81.07(14)
O(6)–Al(2) –O(10)	2	85.11(18)
O(6)–Al(2) –O(11)	2	89.26(19)
O(1)–Al(3) –O(1)′	2	95.17(14)
O(1)–Al(3) –O(7)	4	87.56(19)
O(1)–Al(3) –O(7)′	4	92.44(19)
O(1)–Al(3) –O(8)	2	84.83(14)
O(1)–Al(5) –O(1)′	3	85.46(20)
O(1)–Al(5) –O(2)	6	94.27(14)
O(2)–Al(5) –O(2)′	3	86.00(20)
O(3)–Al(7) –O(3)′	3	96.49(19)
O(3)–Al(7) –O(4)	6	90.50(13)
O(4)–Al(7) –O(4)′	3	81.55(18)
O(4)–Al(9) –O(4)′	3	80.67(18)
O(4)–Al(9) –O(5)	6	89.48(13)
O(5)–Al(9) –O(5)′	3	98.90(19)
O(6)–Al(11)–O(6)′	6	86.54(15)
O(6)–Al(11)–O(6)″	6	93.46(15)
Tetrahedral coordination		
O(1)–Al(4) –O(1)′	3	108.03(18)
O(1)–Al(4) –O(8)	3	110.88(17)
O(2)–Al(6) –O(2)′	3	111.74(17)
O(2)–Al(6) –O(7)	3	107.10(19)
O(6)–Al(10)–O(6)′	3	111.92(15)
O(6)–Al(10)–O(11)	3	106.90(17)
5 coordination		
O(4)–Al(8) –O(4)′	3	119.82(3)
O(4)–Al(8) –O(9)	3	87.54(21)
O(4)–Al(8) –O(10)	3	92.46(21)

TABLE 7
Interatomic Angles of CAM-II

	Number of bonds	Angle (°)
Octahedral coordination		
O(1)–Al(1) –O(1)′	1	101.08(35)
O(1)–Al(1) –O(2)	2	89.53(34)
O(1)–Al(1) –O(9)	2	84.43(48)
O(1)–Al(1) –O(11)	2	100.97(59)
O(2)–Al(1) –O(2)′	1	79.41(23)
O(2)–Al(1) –O(9)	2	91.14(50)
O(2)–Al(1) –O(11)	2	82.23(62)
O(3)–Al(2) –O(3)′	1	86.51(34)
O(3)–Al(2) –O(4)	2	95.03(48)
O(3)–Al(2) –O(12)	2	86.76(46)
O(3)–Al(2) –O(13)	2	97.90(60)
O(4)–Al(2) –O(4)′	1	83.17(28)
O(4)–Al(2) –O(12)	2	89.37(47)
O(4)–Al(2) –O(13)	2	85.82(57)
O(5)–Al(3) –O(5)′	1	79.66(27)
O(5)–Al(3) –O(6)	2	91.30(34)
O(5)–Al(3) –O(10)	2	89.79(53)
O(5)–Al(3) –O(14)	2	86.44(52)
O(6)–Al(3) –O(6)′	1	97.29(31)
O(6)–Al(3) –O(10)	2	85.52(45)
O(6)–Al(3) –O(14)	2	97.70(47)
O(6)–Al(7) –O(6)′	3	96.31(38)
O(6)–Al(7) –O(8)	6	89.80(47)
O(8)–Al(7) –O(8)′	3	83.36(25)
O(1)–Al(8) –O(1)′	3	98.02(41)
O(1)–Al(8) –O(7)	6	90.47(55)
O(7)–Al(8) –O(7)	3	79.58(22)
O(2)–Al(10)–O(2)′	3	85.75(35)
O(2)–Al(10)–O(3)	6	96.01(39)
O(3)–Al(10)–O(3)′	3	82.19(41)
O(4)–Al(11)–O(4)′	3	86.88(40)
O(4)–Al(11)–O(5)	6	92.66(44)
O(5)–Al(11)–O(5)′	3	87.79(42)
Tetrahedral coordination		
O(3)–Al(4) –O(3)′	3	104.68(38)
O(3)–Al(4) –O(9)	3	113.92(33)
O(4)–Al(5) –O(4)′	3	111.58(32)
O(4)–Al(5) –O(10)	3	107.26(35)
O(5)–Al(6) –O(5)′	3	111.86(34)
O(5)–Al(6) –O(12)	3	106.97(38)
O(2)–Al(9) –O(2)′	3	113.30(27)
O(2)–Al(9) –O(13)	3	105.30(33)
5 coordination		
O(7)–Al(12)–O(7)′	3	118.23(20)
O(7)–Al(12)–O(11)	3	97.71(44)
O(7)–Al(12)–O(11)′	3	82.29(44)
O(8)–Al(13)–O(8)′	3	118.87(40)
O(8)–Al(13)–O(14)	3	83.9(11)
O(8)–Al(13)–O(14)′	3	96.1(11)

hedra, 12-coordinated Ca and 5-coordinated Al. Stevels and Schrama-de Pauw (5) assumed the formula to be $CaMg_xAl_{12-2x/3}O_{19}$, which indicates the normal magnetoplumbite structure containing a small amount of vacancy at the Al sites, but in the present study the structures of both compounds are revealed to be more complex than the simple magnetoplumbite structure. The stacking sequence of both compounds are schematically drawn in Fig. 2. Magnetoplumbite structure (denoted as *M* type) is also presented in the figure as a reference, so, in both cases, the enlargement of the spinel block thickness by the insertion of spinel elements is clearly recognized. For CAM-I, every other spinel block is extended making a rhombohedral symmetry with unusually long *c*-axis length; on the other hand, all spinel blocks are extended in the case of CAM-II, resulting in hexagonal symmetry. This kind of stacking sequence has not been reported in the case of

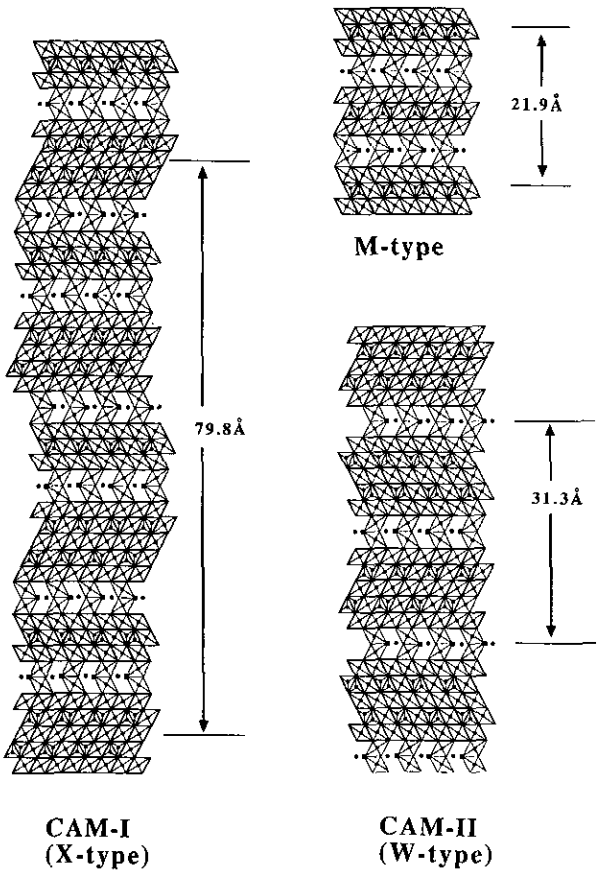

FIG. 2. The structure of CAM-I (X type) and CAM-II (W type) projected on the (110) plane. The c-axis lengths of the unit cells are indicated. For reference, the magnetoplumbite structure (M type) is also shown. Filled rectangles represent the large cations (Ca^{2+}), and filled and open circles are Al ions. Oxygens are not shown but are situated at the end of the bonds expressed in thin lines.

hexaaluminates, but it has been already described and has been thoroughly investigated in the ferrites system (16–20). To understand the sequence, three structure blocks S, M, and Y were usually considered as the elemental structure units (19). These units are combined in a certain ratio and stacked in the c direction forming series of structure groups having a layered structure. S is the stacking element having the spinel structure with a composition of $Mg_2Al_4O_8$, and M represents a typical magnetoplumbite structure unit having a formula $GAl_{12}O_{19}$, which consists of one spinel block and a conduction layer containing a large cation G. The other unit Y, which is expressed as $G_2Mg_2Al_{12}O_{22}$, has a sort of expanded conduction plane with one spinel block. The Y unit can not be observed in the simple magnetoplumbite structure. Combination of these three kinds of elements are known to make a variety of layer structures. The stacking of M leads to the normal magnetoplumbite structure (M type in Fig. 2). So far, two types of combination of structure units are known for hexaferrites (17, 19) as shown in Fig. 3: One is M_nS (n = 1, 2, 3, ..., e.g., MS, M_2S, M_3S, ...) and the other is M_pY_n (p, n = 1, 2, 3, ...). The present compounds CAM-I and CAM-II exhibit, respectively, M_2S and MS stacking, both of which belong to the M_nS type. The former is conventionally expressed as X type and the latter as W type in the hexaferrites system.

The W-type structure usually shows the $P6_3/mmc$ space group, but, in the case of CAM-II, it was assigned to the lower symmetric $P\bar{6}m2$ because of the existence of weak $l = 2n + 1$ reflections for hhl. Probably this is because of the unbalanced distribution of Mg ions in the extended spinel block and/or Ca ions in the conduction layer. Mg ions are known to occupy the tetrahedral site in the middle of the spinel block (21). In the extended spinel block of CAM-II, there are two corresponding Al tetrahedral sites on both sides of the central Al octahedron layer. Though Al and Mg cannot be distinguished by X-ray, it would be

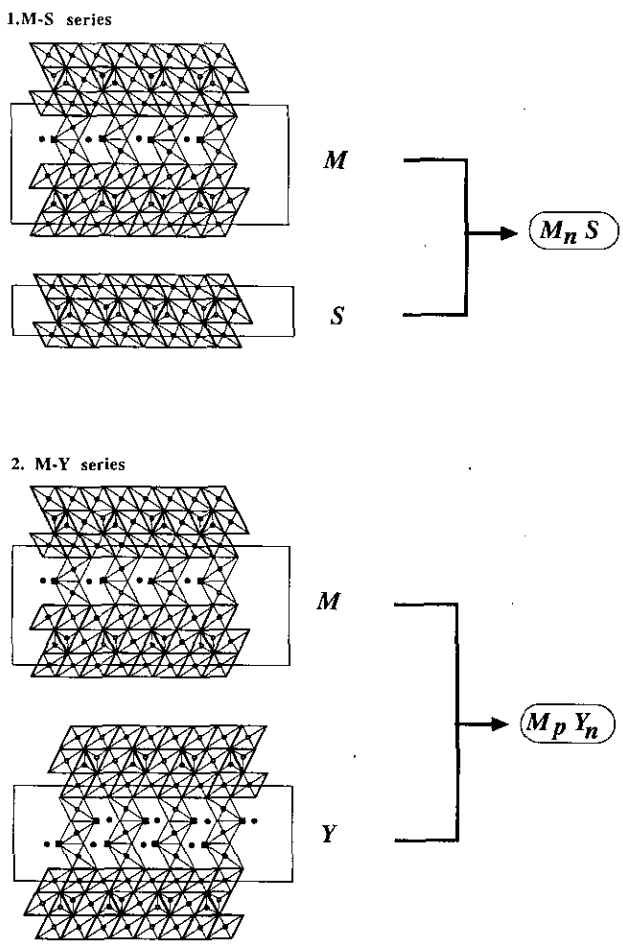

FIG. 3. Schematic representation of two series of polytypic compounds in the magnetoplumbite structure. The marks are the same as in Fig. 2. See Ref. (19).

possible to estimate at which site Mg ions are concentrated since the bond length of Al tetrahedron (ca. 1.80 Å) becomes larger when Al is replaced by Mg. As can be seen in Table 5, the Al(4)–O (average 1.90 Å) and Al(9)–O (average 1.86 Å) distances are much longer than that of Al(5)–O (average 1.83 Å) and Al(6)–O (average 1.79 Å), which indicates the concentration of Mg at the Al(4) and Al(9) sites. On the Ca(1) side, Al(4) and Al(9) tetrahedra are situated and on the Ca(2) side, Al(5) and Al(6) tetrahedra are situated. The tendency of the Ca(1) occupancy to decrease (up to 93%) during the least-squares refinement may be correlated to the Mg distribution. Thus the lower symmetric space group $P\bar{6}m2$ can be attributed to the uneven distribution of Mg in the spinel block and Ca in the conduction plane. Even in this case, the conduction layer should be a mirror plane in a symmetrical sense; however, as can be seen in Fig. 1, the mirror plane symmetry with respect to the conduction layer is seemingly absent because the contrast of the spinel-like blocks on both sides of the conduction layer looks different. This may be due to the effects of plural electron diffraction, which are often observed in the HRTEM data of β- and β'''-alumina-related structures (22).

Structure refinement of the crystal having similar composition $Ca_{0.95}Mg_{0.9}Al_{10.1}O_{17}$ and β''-alumina structure was already published (23). β''-alumina is composed of a normal spinel block and a centrosymmetrical conduction plane which is different from the mirror-symmetrical conduction plane of magnetoplumbite. But this compound was synthesized by the ion-exchange of Na–β''-alumina and is known to be unstable at high temperature with final decomposition into magnetoplumbite (24). As we are dealing with stable compounds which appear in phase diagrams, no further consideration will be given to these kind of compounds.

In the case of Ca–hexaaluminate, only M_nS-type stacking was observed in this study. The stable phases found in this study were those with $n \leqq 2$, but there is possibility that M_nS-type compounds with higher n are yet to be found between CAM-I and $CaAl_{12}O_{19}$. By incorporation of Mg in the spinel block, some hexaaluminates are known to change into a different structure type, which will be discussed in detail in our forthcoming paper.

The obtained compositions for CAM-I and CAM-II exhibit a little bit less Mg than the expected compositions $Ca_2Mg_2Al_{28}O_{46}$ for CAM-I and $CaMg_2Al_{16}O_{27}$ for CAM-II (see Table 1). Our phase diagram study (Part I) showed that there were solid solutions to the Mg-deficient side in both cases by the mechanism $3Mg^{2+} = 2Al^{3+}$ + Vacancy. The compositions of the obtained crystals by the FZ method are situated near the end of the solid solution range to the Mg-deficient side.

ACKNOWLEDGMENT

The authors are very grateful to Mr. K. Kosuda (NIRIM) for help in electron probe microanalysis.

REFERENCES

1. K. Kato and H. Saalfeld, *Neues Jahrb. Mineral. Abh.* **109,** 192 (1968).
2. A. Utsunomiya, K. Tanaka, H. Morikawa, F. Marumo, and H. Kojima, *J. Solid State Chem.* **75,** 197 (1988).
3. A. J. Lindop, C. Matthews, and D. W. Goodwin, *Acta Crystallogr. Sect. B* **31,** 2940 (1975).
4. N. Iyi, S. Takekawa, and S. Kimura, *J. Solid State Chem.* **83,** 8 (1989).
5. A. L. N. Stevels and A. D. M. Schrama-de Pauw, *J. Electrochem. Soc.* **123,** 691 (1976).
6. R. V. Kumar and D. A. R. Kay, *Metall. Trans. B* **16,** 107 (1985).
7. D. J. Fay and R. V. Kumar, *Scand. J. Metall.* **22,** 266 (1993).
8. M. Göbbels, E. Woermann, and J. Jung, *J. Solid State Chem.*, in press.
9. S. Kimura and I. Shindo, *J. Crystal Growth* **41,** 192 (1977).
10. Y. Matsui, S. Horiuchi, Y. Bando, Y. Kitami, M. Yokoyama, S. Suehara, I. Matsui, and T. Katsuta, *Ultramicroscopy* **39,** 8 (1991).
11. J. A. Ibers and W. C. Hamilton, "International Tables for X-ray Crystallography, Vol. 4." Kynoch Press, Birmingham, 1974.
12. T. Sakurai, K. Nakatsu, H. Iwasaki, and M. Fukuhara, "RSFLS-4, UNICS II." Crystallographic Society of Japan, 1967.
13. T. Sakurai, "RSSFR-5, UNICS II." Crystallographic Society of Japan, 1967.
14. P. J. Becker and P. Coppens, *Acta Crystallogr. Sect. A* **30,** 148 (1974).
15. P. J. Becker and P. Coppens, *Acta Crystallogr. Sect. A* **30,** 129 (1974).
16. P. B. Braun, *Philips Res. Rep.* **12,** 491 (1957).
17. J. A. Kohn and D. W. Eckart, *Z. Kristallogr.* **119,** S 454 (1964).
18. R. O. Savage and A. Tauber, *J. Am. Ceram. Soc.* **47,** 13 (1964).
19. J. A. Kohn, D. W. Eckart, and C. F. Cook, Jr., *Science* **172,** 519 (1971).
20. A. Collomb, O. Abdelkader, P. Wolfers, J. C. Guitel, and D. Samaras, *J. Magn. Magn. Mater.* **58,** 247 (1986).
21. G. Collin, R. Comes, J. P. Boilot, and Ph. Colomban, *Solid State Ionics* **1,** 59 (1980).
22. Y. Matsui, Y. Bando, Y. Kitami, and J. L. Hutchison, *J. Electron Microsc.* **35,** 395 (1986).
23. M. Aldén, J. O. Thomas, and G. C. Farrington, *Acta Crystallogr. Sect. C* **40,** 1763 (1984).
24. A. Petric, private communication, 1988.